Dornieden et al. Supplemental Material

Table of Contents

Supplemental Table 1. Antibodies for phenotypic analysis.

Molecule	Clone	Fluorochrome	Manufacturer	Catalog Number	Panel
CD3	SK7	PerCP/Cy5.5	Biolegend, San Diego, USA	344808	1, 2, 3, 4, 5
CD4	SK3	BUV395	BD, Heidelberg, Germany	563550	1, 2, 3,4 , 5
CD8	SK1	APCeFluor780	Thermo Fisher, Darmstadt, Germany	47-0087-42	1, 2, 3, 4, 5
CD14	63D3	BV510	Biolegend, San Diego, USA	367123	1, 2, 3, 4, 5
CD19	SJ25C1	BV510	Biolegend, San Diego, USA	363019	1, 2, 3, 4, 5
CD25	BC96	PE/Cy7	Biolegend, San Diego, USA	302612	3
CD28	CD28.2	BV711	Biolegend, San Diego, USA	302947	1
CD38	HIT2	BV605	Biolegend, San Diego, USA	303532	2
CD45RA	HI100	BV650	Biolegend, San Diego, USA	304135	1, 3
CD45RO	UCHL1	BV650	Biolegend, San Diego, USA	304231	2, 5
CD49a	TS2/7	PE/Cy7	Biolegend, San Diego, USA	328311	1, 5
CD56	5.1H11	BV785	Biolegend, San Diego, USA	328311	1, 2, 4
CD62L	DREG-56	BV605	BD, Heidelberg, Germany	562719	1, 3
CD69	FN50	Alexa700	Biolegend, San Diego, USA	310922	1, 2
CD69	FN50	BV711	Biolegend, San Diego, USA	310943	3
CD69	FN50	FITC	Biolegend, San Diego, USA	310903	4, 5
CD103	Ber-ACT8	BV785	Biolegend, San Diego, USA	350229	5
CD103	Ber-ACT8	PE	Biolegend, San Diego, USA	350206	1, 2, 3, 4
CD161	HP-3G10	PE/Dazzle594	Biolegend, San Diego, USA	339940	2, 3, 5
CTLA4	BNI3	BV421	Biolegend, San Diego, USA	369605	3
FoxP3	150D	Alexa647	Biolegend, San Diego, USA	320014	3
HLA-DR	L243	FITC	Biolegend, San Diego, USA	307604	3
HLA-DR	L243	PE/Cy7	Biolegend, San Diego, USA	307615	2
Ki67	B56	Alexa700	BD, Heidelberg, Germany	561277	3, 5
L/D	-	Aqua (BV510)	Biolegend, San Diego, USA	423101	1, 2, 3, 4, 5
NKG2D	1D11	BV421	Biolegend, San Diego, USA	320822	1, 2
PD1	EH12.1	BV711	BD, Heidelberg, Germany	564017	2
Tox	REA473	APC	Miltenyi, Bergisch Gladbach, Germany	130-118-474	4
Vα7.2	3C10	APC	Biolegend, San Diego, USA	351708	1, 2
Vα7.2	3C10	BV711	Biolegend, San Diego, USA	351731	5

Supplemental Table 2. Multimers.

Virus	Allele	Peptide	Antigen	Catalog Number
CMV	HLA-A*0201	NLVPMVATV	pp65	WB2132-PE
Influenza	HLA-A*0201	GILGFVFFL	MP	WB2161-PE
BKV	HLA-A*0201	LLMWEAVTV	VP1	WB2687-PE
EBV	HLA-A*0201	GLCTLVAML	BMLF1	WB2130-PE

Supplemental Table 3. Antibodies for phenotypic analysis of antigen-specific $CD8^+$ T cells.

Molecule	Clone	Fluorochrome	Manufacturer	Catalog Number
CD3	SK7	PerCP/Cy5.5	Biolegend, San Diego, USA	344808
CD4	SK3	BUV395	BD, Heidelberg, Germany	563550
CD8	SK1	APCeFluor780	Thermo Fisher, Darmstadt, Germany	47-0087-42
CD14	63D3	BV510	Biolegend, San Diego, USA	367123
CD19	SJ25C1	BV510	Biolegend, San Diego, USA	363019
CD45RA	HI100	BV650	Biolegend, San Diego, USA	304135
CD62L	DREG-56	BV605	BD, Heidelberg, Germany	562719
CD69	FN50	Alexa700	Biolegend, San Diego, USA	310922
CD103	Ber-ACT8	BV785	Biolegend, San Diego, USA	350229
CTLA4	BNI3	BV421	Biolegend, San Diego, USA	369605
HLA-A2	BB7.2	APCCy7	Biolegend, San Diego, USA	343310
HLA-DR	L243	PE/Cy7	Biolegend, San Diego, USA	307615
L/D	-	Aqua (BV510)	Biolegend, San Diego, USA	423101
PD1	EH12.1	BV711	BD, Heidelberg, Germany	564017

Supplemental Table 4. Antibodies for functional analysis.

Molecule	Clone	Fluorochrome	Manufacturer	Catalog Number
CD3	SK7	PerCP/Cy5.5	Biolegend, San Diego, USA	344808
CD4	SK3	BUV395	BD, Heidelberg, Germany	563550
CD8	SK1	APCeFluor780	Thermo Fisher, Darmstadt, Germany	47-0087-42
CD14	63D3	BV510	Biolegend, San Diego, USA	367123
CD19	SJ25C1	BV510	Biolegend, San Diego, USA	363019
CD45RO	UCHL1	BV650	Biolegend, San Diego, USA	304231
CD49a	TS2/7	PE/Cy7	Biolegend, San Diego, USA	328311
CD69	FN50	BV711	Biolegend, San Diego, USA	310943
CD103	Ber-ACT8	PE	Biolegend, San Diego, USA	350206
CD161	HP-3G10	PE/Dazzle594	Biolegend, San Diego, USA	339940
GranzymeB	GB11	FITC	Biolegend, San Diego, USA	515403
IFN-γ	4S.B3	eFluor450	Thermo Fisher, Darmstadt, Germany	48-7319-42
IL-2	MQ1-17H12	BV605	Biolegend, San Diego, USA	500332
IL-17	BL168	BV785	Biolegend, San Diego, USA	512338
L/D	-	Aqua (BV510)	Biolegend, San Diego, USA	423101
TNFα	MAb11	Alexa700	Biolegend, San Diego, USA	502928
Vα7.2	3C10	APC	Biolegend, San Diego, USA	351708

Supplemental Table 5. Antibodies for MELC histology.

Molecule	Clone	Fluoro-chrome	Manufacturer	Catalog Number
AQP2 (E-2)		PE	Santa Cruz Biotechnology, Dallas, USA	sc-515770PE
CD3	REA613	PE	Miltenyi, Bergisch Gladbach, Germany	130-113-139
CD4	VIT4	PE	Miltenyi, Bergisch Gladbach, Germany	130-113-776
CD8	BW135/80	PE	Miltenyi, Bergisch Gladbach, Germany	130-113-720
CD11c	MJ4-27G12	PE	Miltenyi, Bergisch Gladbach, Germany	130-114-106
CD14	Tük4	PE	Miltenyi, Bergisch Gladbach, Germany	130-113-709
CD16	REA423	PE	Miltenyi, Bergisch Gladbach, Germany	130-113-955
CD31	9G11	PE	R&D Systems, Minneapolis, USA	FAB3567P
CD45RA	REA562	PE	Miltenyi, Bergisch Gladbach, Germany	130-098-184
CD45RO	UCHL1	PE	DRFZ, Berlin, Germany	
CD49a	TS2/7	PE	Biolegend, San Diego, USA	328303
CD56	AF12-7H3	PE	Miltenyi, Bergisch Gladbach, Germany	130-098-137
CD69	REA824	PE	Miltenyi, Bergisch Gladbach, Germany	130-112-613
CD103	Ber-ACT8	PE	Miltenyi, Bergisch Gladbach, Germany	130-103-709
CD161	191B8	PE	Miltenyi, Bergisch Gladbach, Germany	130-114-119
CD163	RM3/1	PE	Biolegend, San Diego, USA	326505
DAPI			Thermo Fisher, Darmstadt, Germany	D1306
HLA-DR	REA332	PE	Miltenyi, Bergisch Gladbach, Germany	130-120-784
Ki67	MIB1	FITC	Dako, Glostrup, Denmark	F7268
TCR Vα7.2	3C10	PE	Biolegend, San Diego, USA	351705

Supplemental Table 6. Used statistics.

Figure	Statistic test
1 B-D	two-tailed paired T test / Wilcoxon Signed Ranks test
2 B	two-tailed Wilcoxon Signed Ranks test
3 B-C	One-way ANOVA (with multiple comparison corrected by the Tukey's method) / Friedman test (with multiple comparison corrected by the Dunn's method)
3 D	Spearman's rank-order coefficients
3 E	Ordinary One-way ANOVA (with multiple comparison corrected by the Tukey's method) / Kruskal-Wallis test (with multiple comparison corrected by the Dunn's method) Spearman's rank-order coefficients
4 A	two-tailed Wilcoxon Signed Ranks test
5B, F	two-tailed paired T test / Wilcoxon Signed Ranks test
6 A, B, D	two-tailed paired T test / Wilcoxon Signed Ranks test
7 B, C	two-tailed paired T test / Wilcoxon Signed Ranks test
7 D	two-tailed unpaired T test / Mann-Whitney test
8 B	Kruskal-Wallis test (with multiple comparison corrected by the Dunn's method)
8 C-D	One-way ANOVA (with multiple comparison corrected by the Tukey's method) Friedman test (with multiple comparison corrected by the Dunn's method)
Suppl. 3 A, B	two-tailed paired T test / Wilcoxon Signed Ranks test
Suppl. 5 A, B	two-tailed paired T test / Wilcoxon Signed Ranks test
Suppl. 6 B	two-tailed paired T test / Wilcoxon Signed Ranks test
Suppl. 7 A, B, C	two-tailed paired T test / Wilcoxon Signed Ranks test
Suppl. 8A	two-tailed unpaired T test / Mann-Whitney test
Suppl. 8 B, C, D	Spearman's rank-order coefficients
Suppl. 14	two-tailed paired T test

Supplemental Figure 1

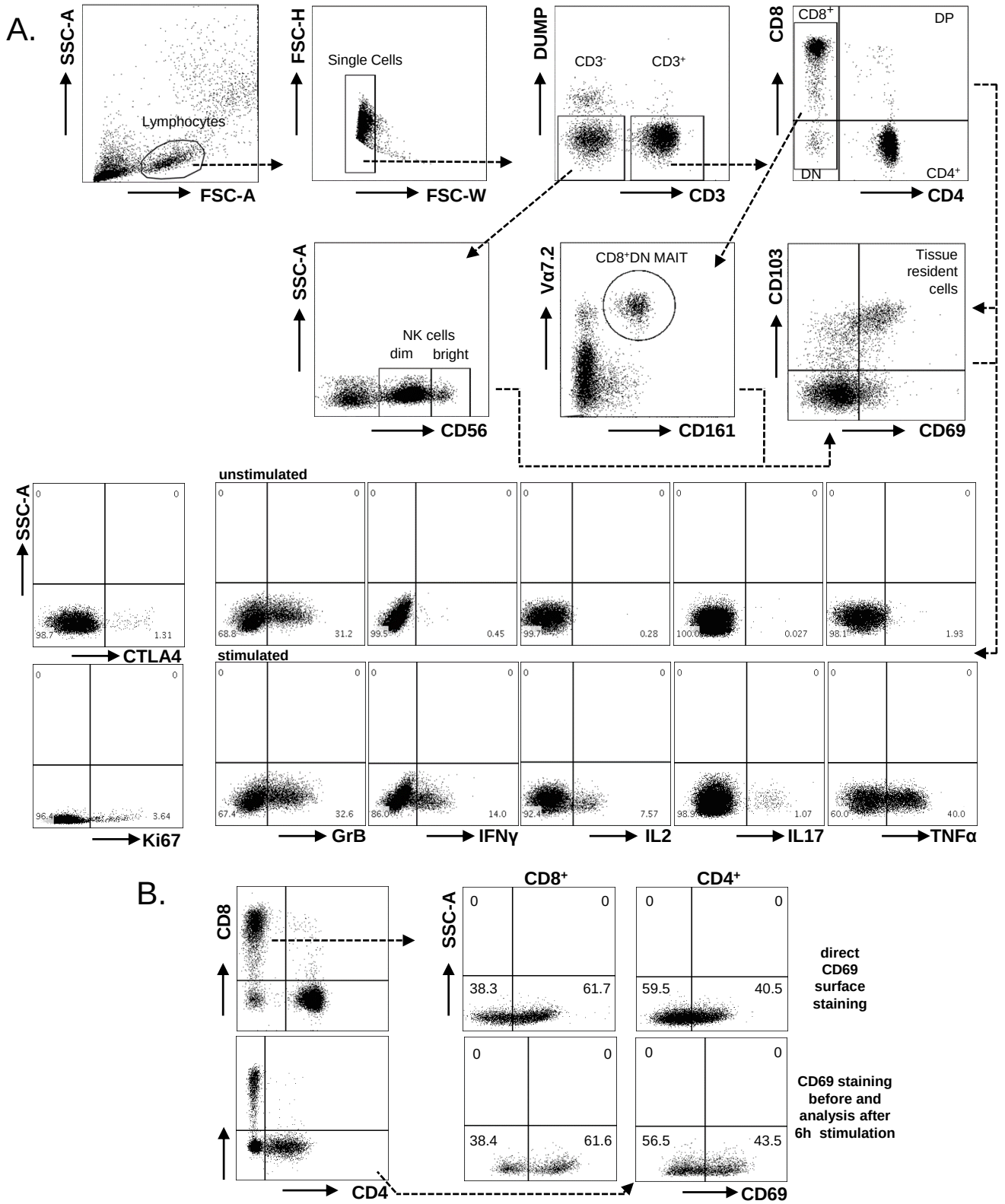

Supplemental Figure 1: (A) *Gating Strategy.* Cells were detected by after gating on single, live $CD14^{-}CD19^{-}$ ("DUMP" negative) lymphocytes. Conventional $CD4^{+}$ and $CD8^{+}$ T cells and $CD8^{+}/CD8^{-}CD4^{-}$("DN") $CD161^{+}V\alpha7.2^{+}$ MAIT cells were identified within the $CD3^{+}$ population. CD56 dim or bright NK cells were identified within the $CD3^{-}$ subset. Tissue resident cells were subsequently detected by single- or co-expression of CD69 and CD103, respectively. Exemplary dot plots for intracellular markers (CTLA4, Ki67) and cytokines (granzyme B (GrB), IFNγ, IL-2, IL-17, TNFα) (B) *Ex vivo staining of CD69 prior to stimulation.* PBMCs were stained with anti-CD69 before culture, thereby preventing its stimulus-dependent increase by PMA/Ionomycin. Plots demonstrate stable staining after 6h activation as compared to the *ex vivo* control.

Supplemental Figure 2

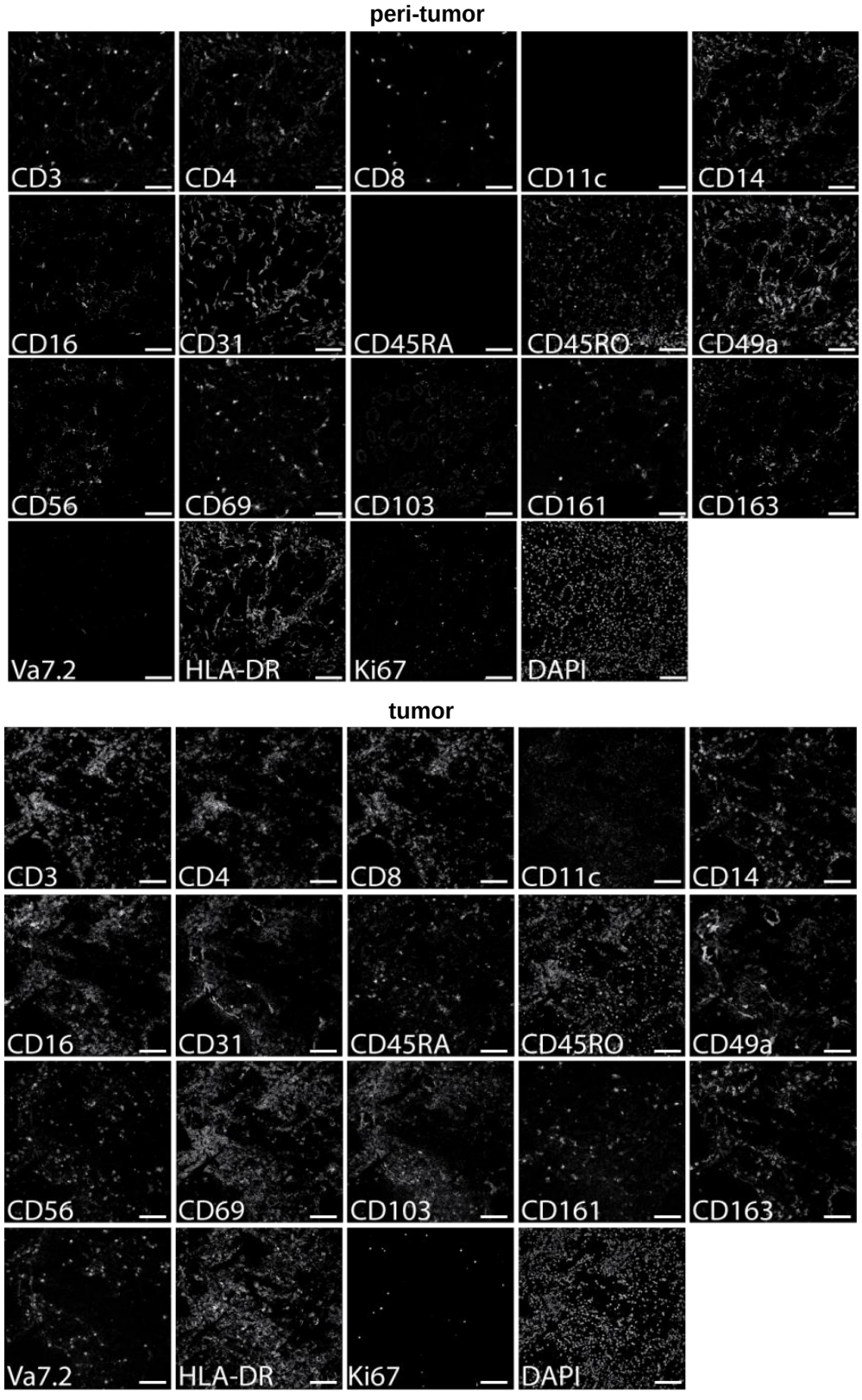

Supplemental Figure 2: Panel overview of a 19 marker MELC run in human kidneys show different degree of T cell infiltration. 2 exemplary different data-sets are shown: 1 peri-tumor samples (A) and 1 tumor samples (B). Each image shows the same field of view, sequentially stained with the depicted fluorescence-labelled antibodies. Images contain 2024 x 2024 pixels and are generated using an inverted wide-field fluorescence microscope with a 20x objective, a lateral resolution of 325 nm and an axial resolution above 5 µm. Scale bar: 100 µm.

Supplemental Figure 3

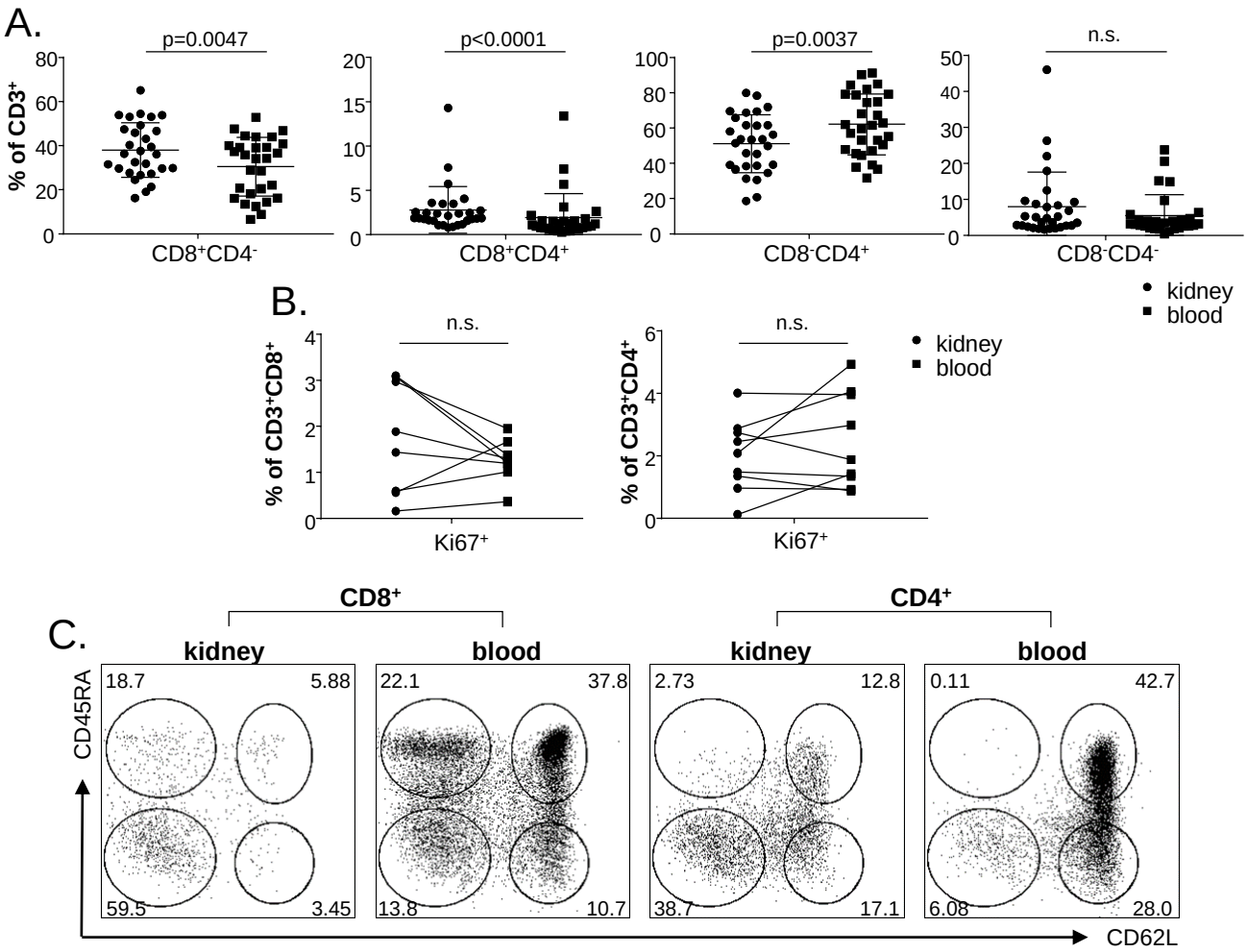

Supplemental Figure 3: (A) *Quantification of PBMC- and tissue-derived T cell subsets.* Frequencies of $CD8^+CD4^-$, $CD8^+CD4^+$, $CD8^-CD4^+$ and $CD8^-CD4^-$ T cells within the $CD3^+$ cell population isolated from paired blood and peri-tumor kidney samples (n=29) were analyzed by FACS. (B) *Ex vivo proliferation of $CD8^+$ and $CD4^+$ T cells.* Proliferation as reflected by Ki67 expression of $CD8^+$ (n=8) and $CD4^+$ (n=9) T cells derived from paired blood and peri-tumor kidney samples. Statistically significant differences were tested with two-tailed paired T or two-tailed Wilcoxon Signed Ranks test and presented as mean values ± SD. (C) Exemplary dot plots for blood and peri-tumor kidney-derived $CD8^+$ and $CD4^+$ T cell subsets according to their CD62L and CD45RA expression.

Supplemental Figure 4

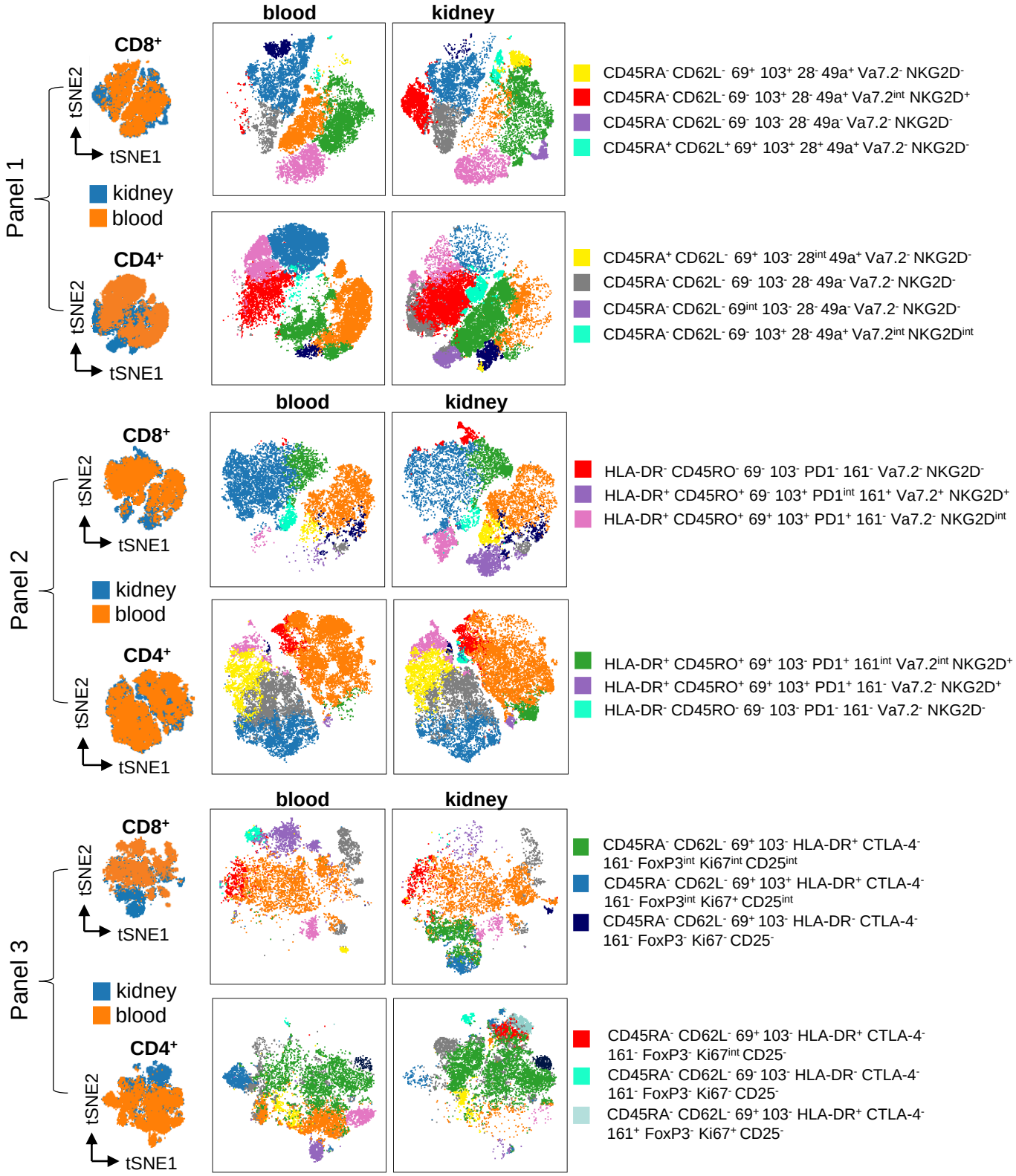

Supplemental Figure 4: *viSNE and FlowSOM analysis of FACS data.* viSNE plots of flow cytometric analysis of viable CD8$^+$ and CD4$^+$ T cells illustrate the separate clustering of kidney and blood. FlowSOM analysis clusters cells into cell subsets based on their marker expression patterns used in the corresponding FACS panels. Only metaclusters identified in kidney but not present in blood are annotated. Markers used for dimensional reduction were identical to those in Figure 1A for the respective panels. [Panel 1: CD103, CD28, CD45RA, CD49a, CD62L, CD69, NKG2D, Va7.2 HLA-DR/PD-1; Panel 2: CD103, CD161, CD45RO, CD69, HLA-DR, NKG2D, PD1, Va7.2; Panel 3: CD103, CD161, CD25, CD45RA, CD62L, CD69, CTLA-4, FoxP3, HLA-DR, Ki67].

Supplemental Figure 5

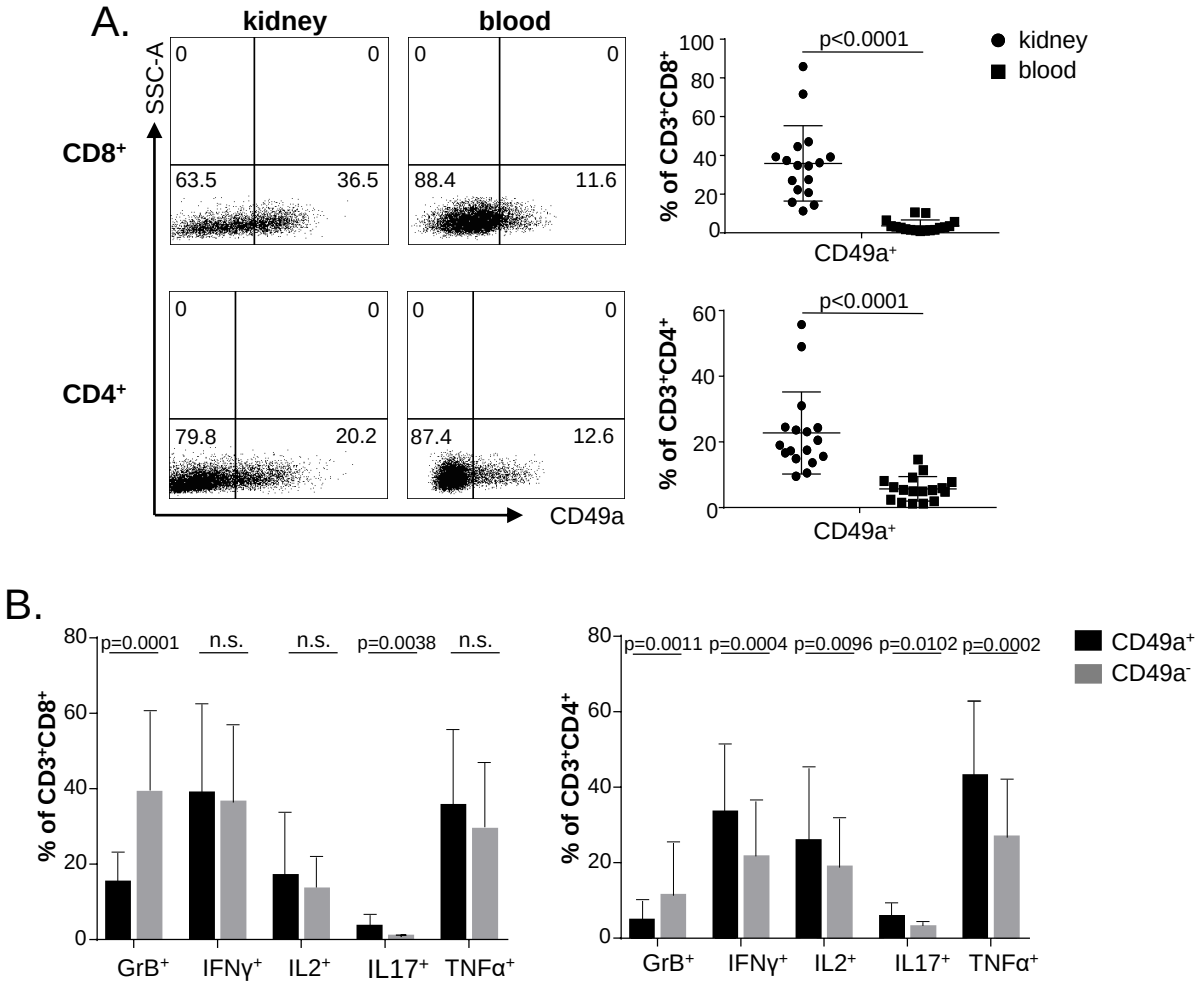

Supplemental Figure 5: (A,B) *CD49a expression and related cytokine profiles.* Exemplary dot plots showing frequencies of CD49a expressing $CD8^+$ and $CD4^+$ T cells in peri-tumor tissue and blood (n=17) (A) and the associated effector molecule profile (Granzyme B, IFNγ, IL-2, IL-17, TNFα) within kidney (n=17) (B). Statistically significant differences were tested with two-tailed paired T or two-tailed Wilcoxon Signed Ranks test and presented as mean values ± SD.

Supplemental Figure 6

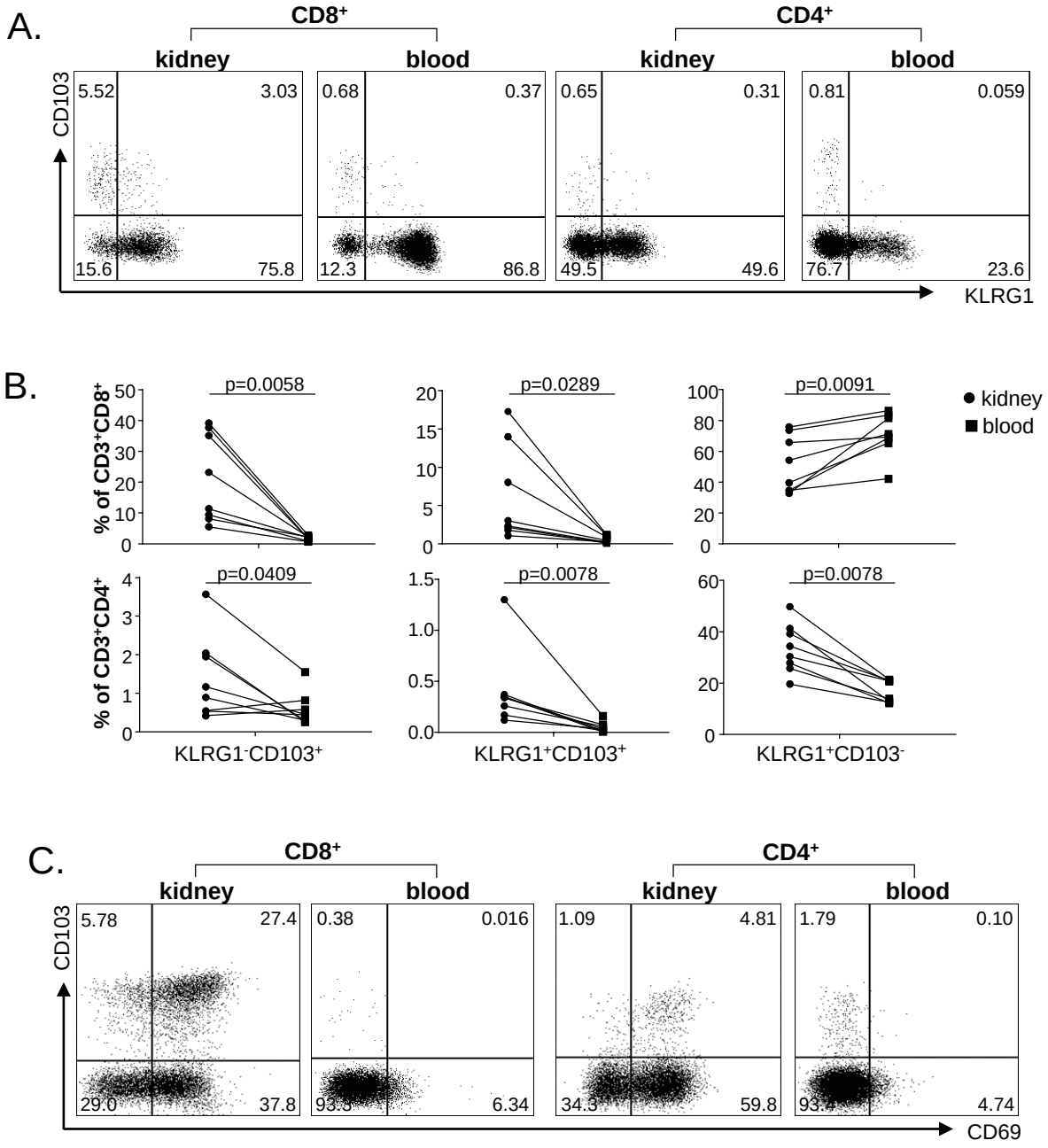

Supplemental Figure 6: (A,B) *KLRG1 and CD103 expression of CD8⁺ and CD4⁺ T cells.* Exemplary dot plots and frequencies for blood and peri-tumor kidney tissue derived CD8⁺ and CD4⁺ T cell subsets according to their KLRG1 and CD103 expression (n=8). Statistical analysis was performed using two-tailed paired T or two-tailed Wilcoxon Signed Ranks test. (C) Exemplary dot plots for blood and peri-tumor kidney-derived CD8⁺ and CD4⁺ T cell subsets expressing CD103 and CD69.

Supplemental Figure 7

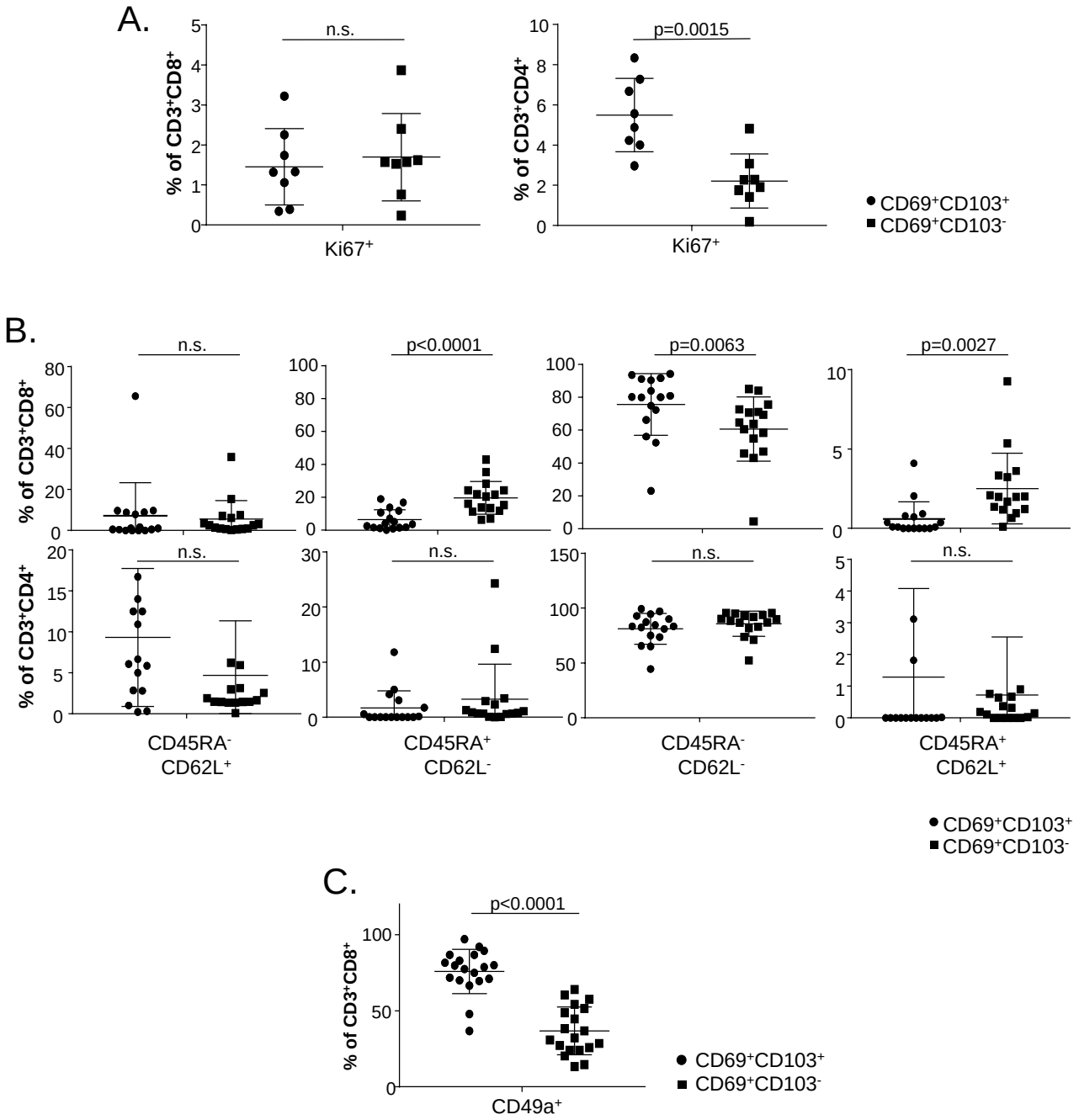

Supplemental Figure 7: (A) *Ex vivo proliferation of CD8⁺ and CD4⁺ T_{RM} cell subsets.* Proliferation status as reflected by Ki67 expression of CD8⁺ and CD4⁺ CD69⁺CD103⁺ and CD69⁺CD103⁻ T cells derived from renal peri-tumor tissue (n=8) was analyzed by FACS. Statistical analysis was performed using two-tailed paired T or two-tailed Wilcoxon Signed Ranks test. (B) *Memory subsets within CD8⁺ and CD4⁺ T_{RM} T cell subsets.* Frequencies of CD45RA⁻CD62L⁺ central memory (T_{CM}), CD45RA⁺CD62L⁻ terminally differentiated effector (T_{EMRA}), CD45RA⁻CD62L⁻ effector memory (T_{EM}) and CD45RA⁺CD62L⁺ naïve cells within CD8⁺ and CD4⁺ T_{RM} peri-tumor kidney T cell subsets CD69⁺CD103⁺ and CD69⁺CD103⁻ (n=16). Statistically significant differences were tested with two-tailed paired T or two-tailed Wilcoxon Signed Ranks test. (C) CD49a expression on renal-derived CD69⁺CD103⁺ and CD69⁺CD103⁻ CD8⁺ T cells (n=19). Statistically significant differences were tested with the Wilcoxon Signed Ranks test and presented as mean values ± SD.

Supplemental Figure 8

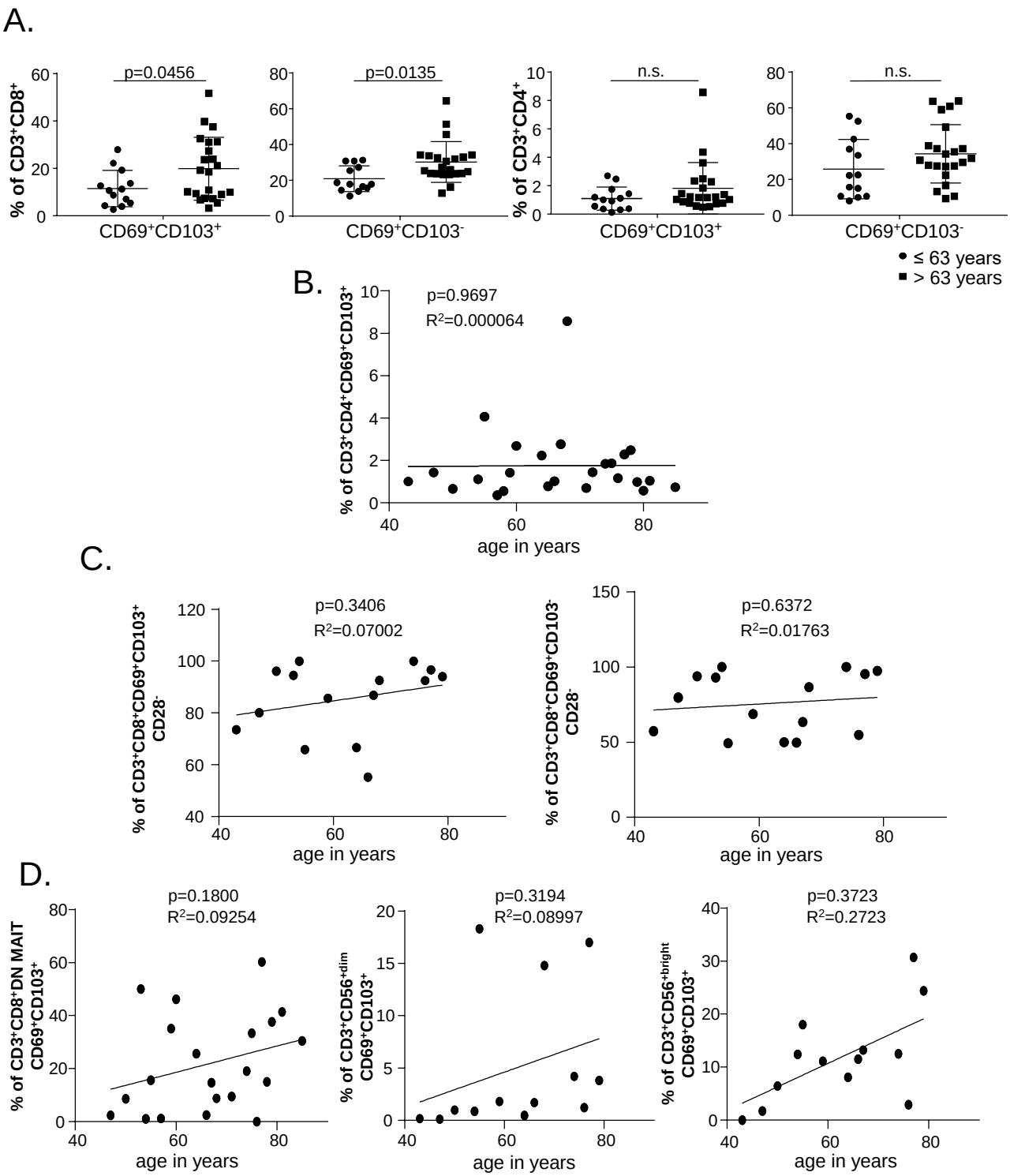

Supplemental Figure 8. (A) Patients were divided into two groups according to the calculated mean age of 63 years (n=35). Group I included patients ≤ 63 years (n=13), whereas Group II included patients > 63 years (n=22). $CD69^+CD103^+$ and $CD69^+CD103^-$ $CD8^+$ and $CD4^+$ T cell frequencies in peri-tumor tissue were compared between the two groups. Statistically significant differences were tested with two-tailed unpaired T or the Mann-Whitney test and presented as mean values ± SD. (B-D) *Correlation of T_{RM} cell subsets and age.* Correlation analysis of (A) $CD4^+CD69^+CD103^+$ T cells (n=35), (B) $CD8^+CD69^+CD103^+CD28^-$ and $CD8^+CD69^+CD103^-CD28^-$ (n=18), and (C) $CD69^+CD103^+$ $TCRV\alpha7.2^+CD161^+$ MAIT (n=27), $CD56^{dim}$ and $CD56^{bright}$ NK cells (n=18) frequencies with patient age. Linear regression analysis was performed and Spearman's rank-order coefficients were calculated.

Supplemental Figure 9

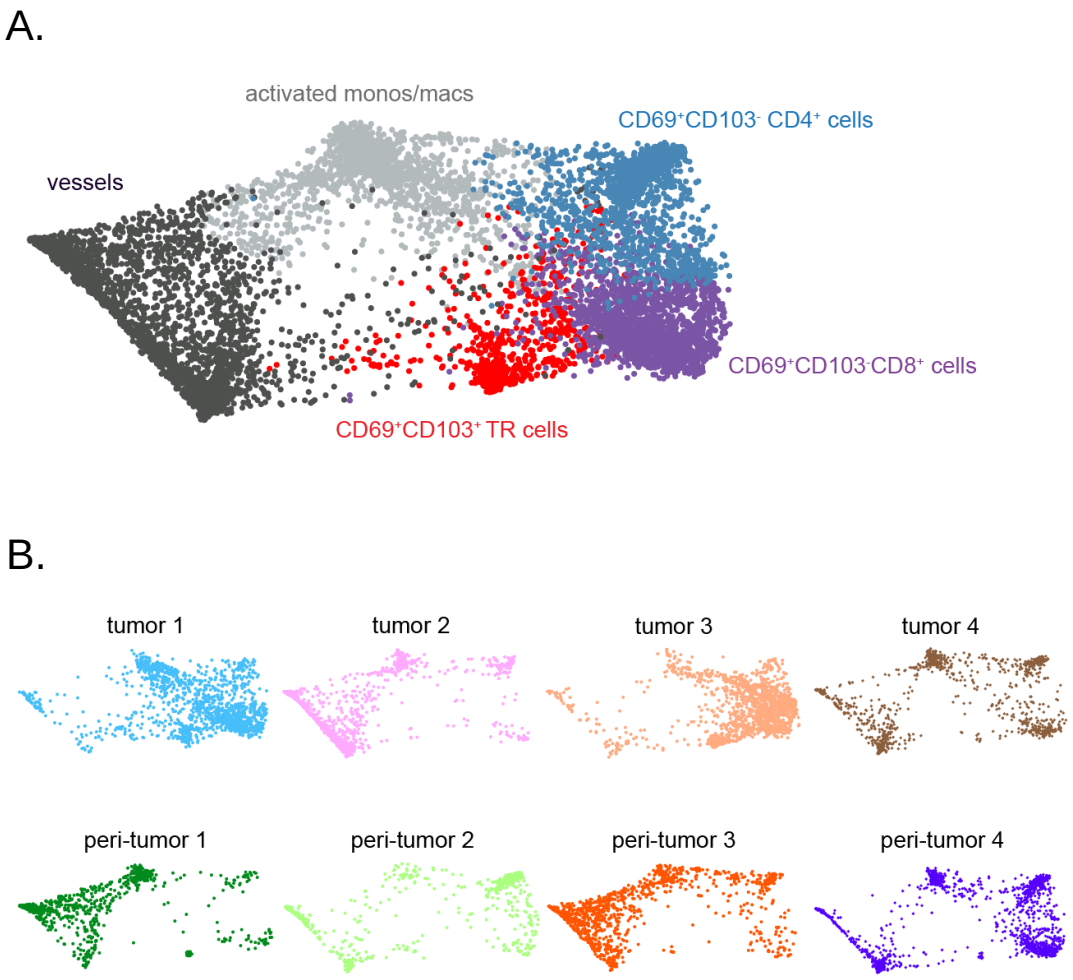

Supplementary Figure 9. *Cluster analysis of MELC data from pooled tumor and patient-matched peri-tumor samples (n=4).* (A) t-SNE maps showing the analysis of 16 measured markers allowing the identification of the following clusters: vessels, activated monocytes/macrophages, $CD69^+CD103^+$ tissue-resident cells, $CD69^+CD103^-CD8^+$ T_{RM} cells, and $CD69^+CD103^-CD4^+$ T_{RM} cells in a color-coded fashion and, (B) a color-code for the individual samples measured, allowing the relation of the cluster to the sample origin.

Supplemental Figure 10

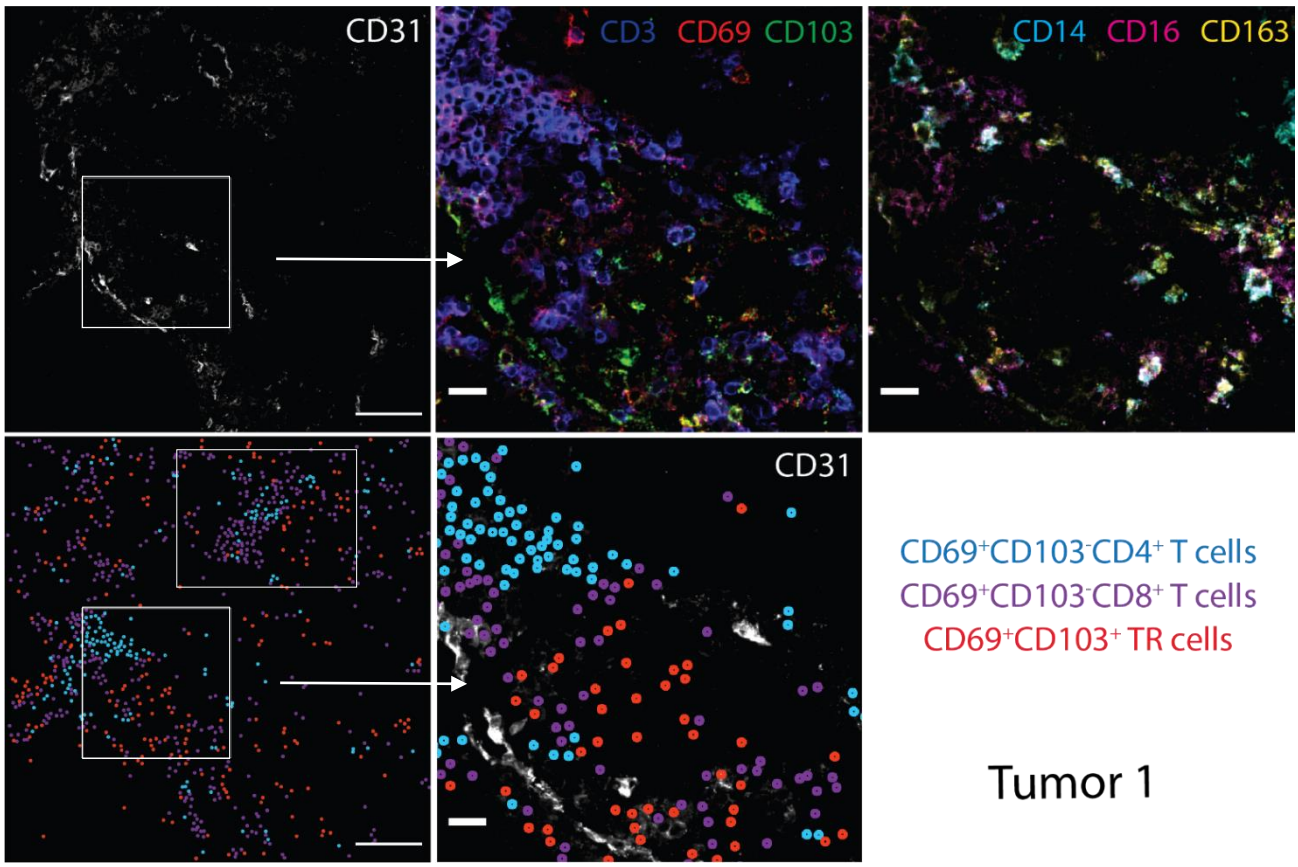

Supplementary Figure 10. *Both, CD69$^+$CD103$^-$ CD4$^+$ and CD69$^+$CD103$^-$ CD8$^+$ T cells form clusters, while and CD69$^+$CD103$^+$ tissue-resident (TR) populations tend to be rather scattered across the tumor tissue. Especially CD69$^+$CD103$^-$ CD4$^+$ T cells could be identified in close proximity to monocyte/macrophages.* Exemplary overlays of MELC fluorescent images depicting endothelial cells (CD31 in white, left panel) and monocyte/macrophages (CD14 in cyan, CD16 in magenta and CD163 in yellow, right panel) together with color-coded dots that represent the centroid spatial coordinates of the three tissue-resident cells clusters identified in (Fig. 6A). The images depict the spatial distribution of the CD69$^+$CD103$^-$CD4$^+$ T cell cluster (light blue dots), the CD69$^+$CD103$^-$CD8$^+$ T cell cluster (purple dots) and the CD69$^+$CD103$^+$ TR cluster (red dots) in each tumor sample and the patient-matched peri-tumor sample analyzed. Figures are representative for n=4 peri-tumor/tumor matched patient samples.

Supplemental Figure 11

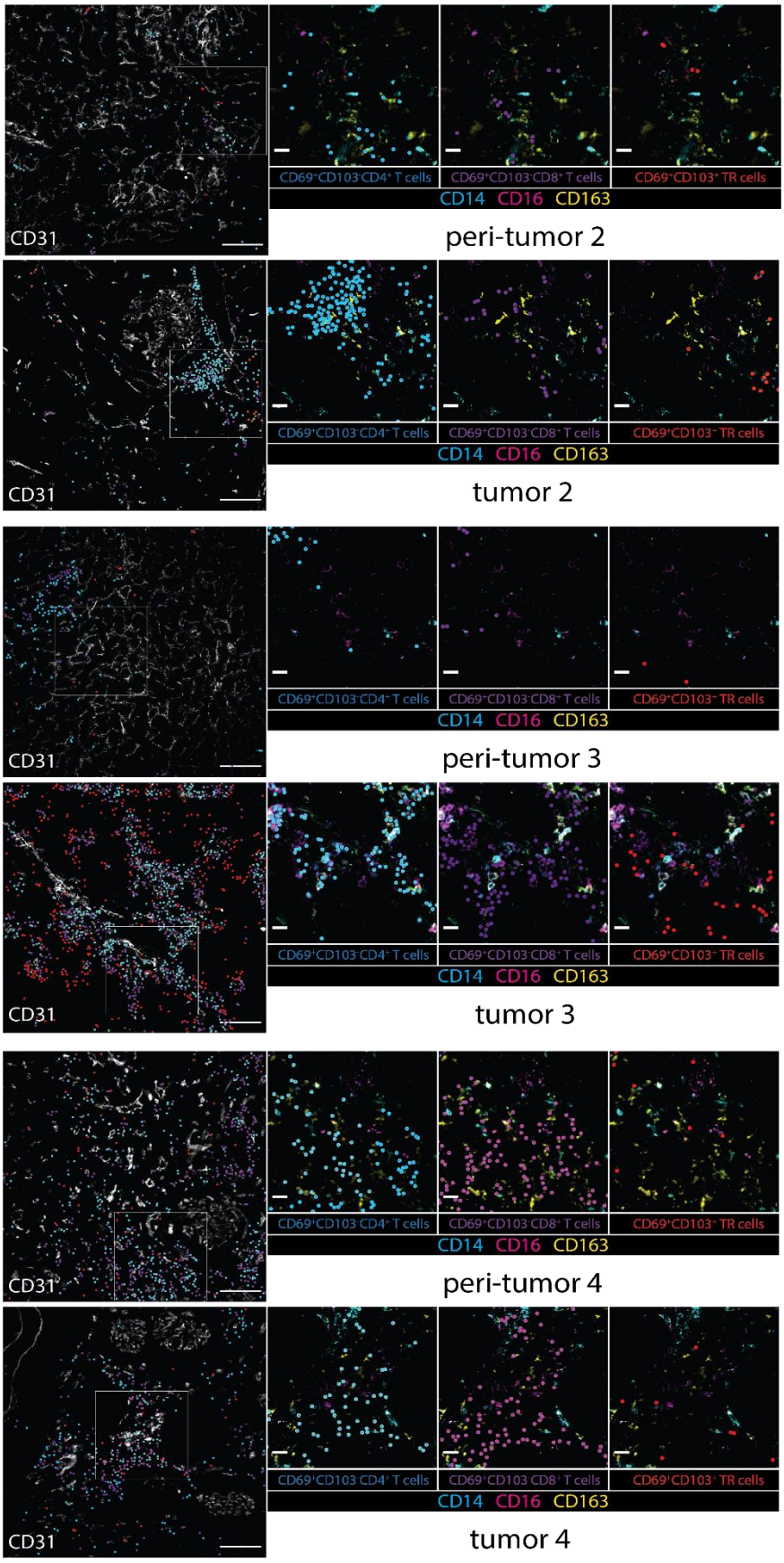

Supplementary Figure 11. Overlays of MELC fluorescent images depicting endothelial cells (CD31 in white, left panel) and monocyte/macrophages (CD14 in cyan, CD16 in magenta and CD163 in yellow, right panel) together with color-coded dots that represent the centroid spatial coordinates of the three tissue-resident cells clusters identified in (Fig. 5A) for n=3 peri-tumor/tumor matched patient samples.

Supplemental Figure 12

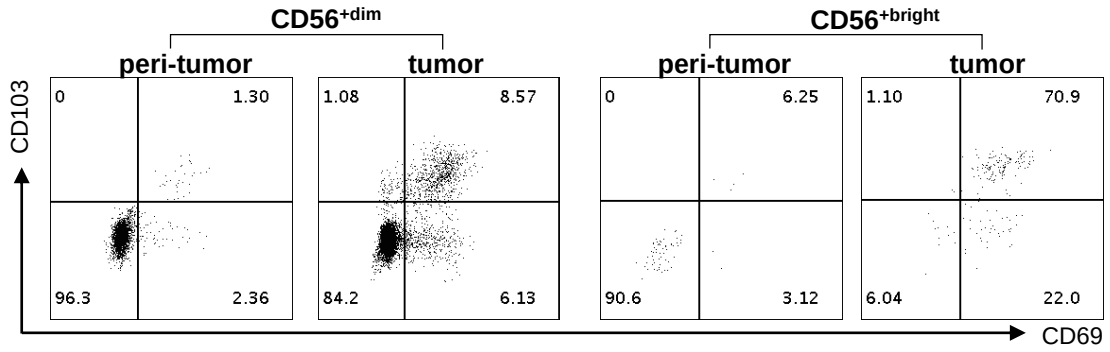

Supplemental Figure 12: *Tissue-residency of NK cells in peri-tumor and tumor kidney tissue.* Exemplary dot plots of CD69 and CD103 expression of $CD56^{+dim}$ and $CD56^{+bright}$ cells isolated from peri-tumor and tumor tissue.

Supplemental Figure 13

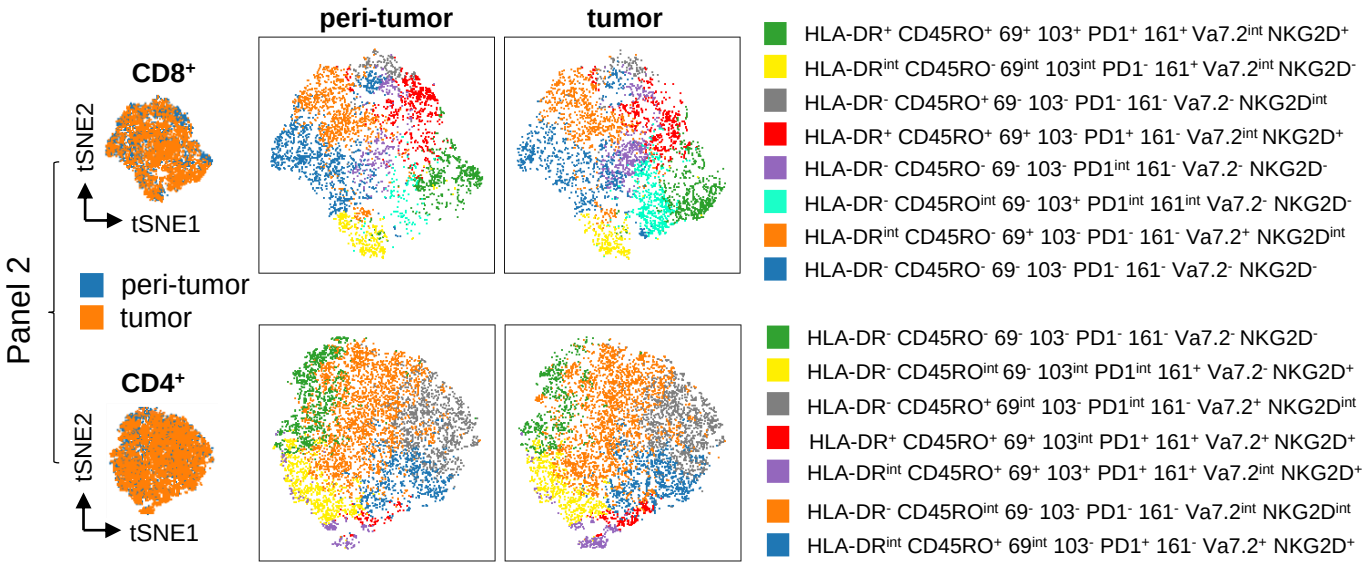

Supplemental Figure 13: *viSNE and FlowSOM analysis of FACS data for peri-tumor and tumor samples.* viSNE plots of flow cytometric analysis of viable $CD8^+$ and $CD4^+$ T cells does not illustrate a separate clustering between peri-tumor and tumor. Main cell clusters identified by FlowSOM analysis are annotated. The markerset from Panel 2 used for dimensional reduction was identical to that in Figure 1A (CD103, CD161, CD45RO, CD56, CD69, HLA-DR, NKG2D, PD-1, Va7.2).

Supplemental Figure 14

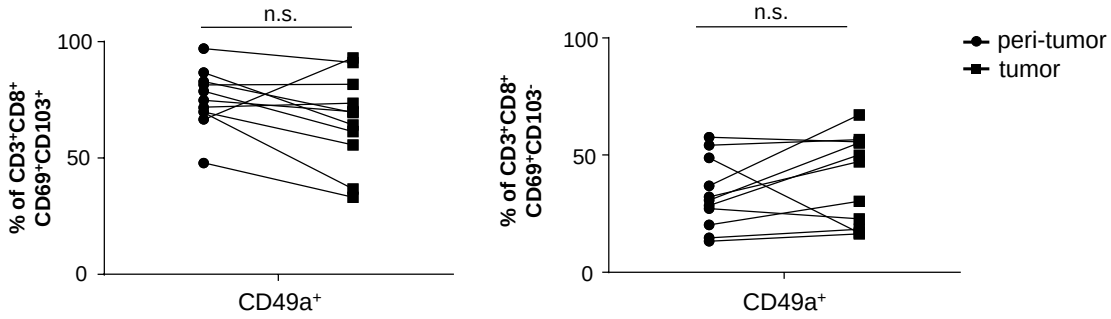

Supplemental Figure 14: *CD49a expression of CD8⁺ T_{RM} T cell subsets.* Frequencies of CD49a expression of CD8⁺ CD69⁺CD103⁺ and CD69⁺CD103⁻ T_{RM} T cells isolated from peri-tumor and tumor tissue (n=11). Statistical analysis was performed using two-tailed paired T test.